Power-Amplifier Characterization Using a Two-Tone Measurement Technique

Christopher J. Clark, Christopher P. Silva, *Fellow, IEEE,* Andrew A. Moulthrop, and Michael S. Muha

***Abstract*—An accurate nonlinear model is necessary to optimize the tradeoff between efficiency and linearity in power amplifiers. Gain compression (AM/AM) and amplitude–phase (AM/PM) distortion are the two primary model inputs used to characterize the nonlinearity. The amplifier's AM/AM and AM/PM characteristics are typically measured statically using a vector network analyzer. Since the input is typically a modulated signal, it is desirable to characterize the amplifier dynamically. This paper describes and demonstrates a dynamic AM/AM and AM/PM measurement and modeling technique involving a spectrum analyzer and two-tone input signals. A complete analysis of the measurement technique is presented, along with the data processing needed for the identification of a new three-box model. The test configuration and procedure are presented with special precautions to minimize measurement error. Results for a solid-state amplifier are used to accurately predict intermodulation distortion, while those for a traveling-wave tube amplifier show good agreement with that obtained dynamically using a 16 quadrature-amplitude-modulation signal.**

***Index Terms*—AM/AM and AM/PM, dynamic modulated signals, high-power amplifiers, intermodulation distortion, nonlinear blackbox modeling, two-tone measurements.**

I. Introduction

MICROWAVE transmitters generally rely on a nonlinear power amplifier as the final amplification stage. Traveling-wave tube amplifiers (TWTAs) are commonly used in satellites [1], while solid-state amplifiers (SSAs) are used for portable wireless communications [2]. Operating these power amplifiers at or near saturation improves power efficiency compared to linear operation, but signal distortion is generally increased. Since power efficiency is critical for both satellite and handheld applications, accurate nonlinear characterization is required. The two major nonlinear distortions can be described in terms of AM/AM and AM/PM conversion characteristics, and these are often used in communication systems modeling [3]. These models are important for predicting end-to-end link performance, as well as simulating spectral regrowth [4]–[6].

An amplifier's AM/AM and AM/PM characteristics are often obtained with a vector network analyzer (VNA) by measuring the gain and phase as a function of input power. Typically, this is a steady-state or static type of measurement, which may erroneously include the thermal [7] or dc bias [8] effects. For communication signals, the amplitude envelope can vary at a frequency corresponding to the information rate, thus, the AM/AM and AM/PM distortion is occurring dynamically. The simple technique presented here measures the dynamic AM/AM and AM/PM at a modulation rate that is more consistent with actual applications. It is based on the spectrum analyzer measurement of intermodulation products using a two-tone test signal [9]. The results may be used in communication systems models in place of VNA-derived static measurements.

Manuscript received October 25, 2000; revised October 30, 2001.

C. J. Clark is with the Multilink Technology Corporation, Santa Monica, CA 90405 USA (e-mail: cclark@mltc.com).

C. P. Silva, A. A. Moulthrop, and M. S. Muha are with The Aerospace Corporation, Los Angeles, CA 90009-2957 USA (e-mail: chris.p.silva@aero.org).

Publisher Item Identifier S 0018-9480(02)05222-5.

II. Nonlinear Amplifier Modeling

There are three basic approaches to amplifier nonlinear modeling, i.e., physics based, circuit based, or blackbox based. The former two methods use device physics to develop either the transport/electromagnetic equations or a lumped/distributed circuit simulation model that must be simulated to determine the amplifier's nonlinear input/output behavior. The circuit-model approach has dominated the characterization of SSAs [10], [11]. For TWTAs, the circuit-model approach has been extensively employed for practical design, whereas the simulation of its characteristic electromagnetic equations can require many hours of CPU time to solve, even on advanced supercomputers. In systems-level modeling, blackbox approaches are often used where a topological configuration of linear/nonlinear components is constructed to replicate the amplifier's overall input/output behavior for a constrained class of signals. The boxes are derived from input/output measurements of the device, whereas their topological configuration stems from computational efficiency and intuition about the amplifier's internal workings. This approach can be implemented using commercially available software.[1,2] Although these models do not employ formal nonlinear system identification principles, systems-level modeling is dominated by this approach because of its relative ease compared to more rigorous alternatives. This paper presents a modest extension of blackbox amplifier models that can provide more accurate predictions for moderately broad-band modulated signals.

Blackbox modeling approaches assume that the nonlinear amplifier provides a causal operator mapping (memoryless or with memory) between the input signal and the output response that can be expressed formally as

$$y(t) = F\left[u(\tau), t - T_m \le \tau \le t\right] \tag{1}$$

where $u(\cdot)$ is the input signal, $y(t)$ is the output response at time t, $F[\cdot]$ represents the operator mapping, and T_m designates the

[1]*SPW, Signal Processing Worksystem*, Cadence Design Systems, San Jose, CA.

[2]*Advanced Design System*, Agilent EESof EDA, Agilent Technologies, HP EESof Div., Hewlett-Packard, Westlake Village, CA 91362.

memory of the power amplifier. All blackbox models and formal nonlinear system identification techniques seek to approximate F for a pertinent or general class of input signals u. In the latter case, F is usually expanded as a integro-operator series that extends the standard convolution representation for linear systems to the nonlinear case. The terms of these expansions are obtained from carefully designed input/output measurements and often involve intensive data-reduction procedures.

The majority of current blackbox amplifier models assume a bandpass nonlinearity [12] and are based on one-tone static measurements. This model includes a zonal filter that accounts for the inherent filtering of the higher harmonics within the device. This model is valid for most communications problems where the input signal is narrow-band in comparison to the center frequency. As a consequence, these models rely on the continuity of F with respect to u since they do not formally identify F. However, in the face of broad-band and multicarrier contexts, wherein the actual signal differs considerably from the one used to construct the model, the continuity of F can no longer be used to ensure the model's predictive fidelity.

The simplest blackbox model is the so-called *one-box model*, consisting of a single frequency-independent memoryless [i.e., $T_m = 0$ in (1)] nonlinearity that contains the AM/AM and AM/PM conversions manifested by continuous wave (CW) inputs at a center frequency f_c passing through the amplifier. More formally, if the CW input is given by

$$u(t) = V_i \cos(\omega_c t + \theta_i) \quad \omega_c = 2\pi f_c, \qquad V_i > 0 \tag{2}$$

and θ_i is an arbitrary phase, then the output of this model is given by

$$y(t) = F\big[u(t)\big] = V_o \cos(\omega_c t + \theta_o) \tag{3a}$$

where

$$\left.\begin{array}{ll} V_o = G(V_i) & \text{(AM/AM conversion)} \\ \Delta\theta := \theta_o - \theta_i = \phi(V_i) & \text{(AM/PM conversion)} \end{array}\right\}. \tag{3b}$$

For a general input signal, it is a common practice to recast $u(t)$ in the form of (2) with $V_i = V_i(t)$ and $\theta_i = \theta_i(t)$, resulting in (3a) with $V_o = V_o(t)$ and $\theta_o = \theta_o(t)$, where the conversions G and ϕ in (3b) are applied instantaneously at each time instant.

An instantaneous envelope transfer function can be derived from single-tone AM/AM and AM/PM measurements using a VNA. Since the input is a sinusoid, the VNA AM/AM measurement actually provides the sine-wave steady-state transmittance [13]. In the absence of AM/PM conversion, a transfer function is obtained from the steady-state transmittance by a Chebyshev transformation [14]. When both AM/AM and AM/PM exist, the envelope transfer function is complex. In this case, the real and imaginary steady-state components can be transformed separately, resulting in two instantaneous transfer functions in quadrature. Good simulation results have been achieved using this approach with a variety of nonlinear devices and input signal types [15]. In addition, modifications of this approach have been used to accurately predict spectral regrowth of digitally modulated signals in FET power amplifiers [16].

In order to handle frequency-dependent effects and nonzero memory, the one-box model is augmented with one or two linear filters preceding or surrounding the nonlinearity, respectively,

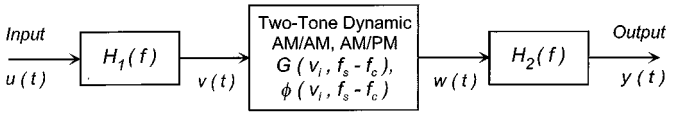

Fig. 1. Three-box nonlinear model based on the two-tone dynamic AM/AM, AM/PM technique, where f_s (f_c) is the frequency of the small tone (large tone).

which essentially shifts the nominal conversions in their abscissa and ordinate axes with frequency. Such models assume that the memory of the amplifier can be adequately captured this way and that the qualitative shape of the conversion curves do not change with frequency. The former assumption is questionable, especially when a general broad-band signal is traced through these models and thought of as being instantaneously a CW tone with some amplitude and phase (as is needed to process the signal through the memoryless nonlinearity). These models predict no interaction between the instantaneous tones, although it is well known that such interaction occurs in a real device because of its finite memory. Likewise, the second assumption is known to be invalid in some amplifiers in which the conversion curves do change shape with frequency. More sophisticated models [17] address the latter inadequacy by replacing the one pair of conversion curves of the memoryless nonlinearity with a finite series of curve pairs, indexed by a finite set of selected frequencies, which are fits to actual measured data.

A. Two-Tone Technique Signal Analysis

The two-tone method of characterizing the nonlinearity is a step in obtaining more accurate nonlinear models. With this method, the transfer functions may be obtained at a rate that corresponds to the modulation envelope, thereby avoiding error due to thermal and dc-bias effects. As will be shown, the two-tone measurement presented here is based on an input signal that can be interpreted as a single large carrier with a small dynamic modulation. Hence, the curves obtained by this technique are termed *dynamic carrier amplitude and phase conversions*.

The blackbox model proposed here is an extension of traditional models based on CW tone measurements to the two-tone case, consisting of a two-tone derived memoryless dynamic AM/AM and AM/PM box sandwiched between two linear filters, as shown in Fig. 1. We will take the memoryless nonlinearity to be referenced to the nominal center frequency of the power amplifier being represented, and assume that the surrounding linear filters can accurately account for the large-tone frequency dependence of the dynamic AM/AM and AM/PM. The change in shape of the dynamic conversions with respect to f_c could be accounted for by curve fitting to measured data [17]. The dependence of the dynamic conversions G and ϕ on the frequency difference $f_s - f_c$, where f_s is the frequency of the small tone, are obtained from measured data. Note that G and ϕ are *envelope* conversions, where $V_i(t)$ denotes the two-tone envelope function. In order to develop a full simulation model from this blackbox topology, one also has to obtain both the amplitude and phases of the two filters. Although procedures for the identification of the complete model will be given, its application will be primarily restricted to the determination of the simpler one-box dynamic AM/AM and AM/PM model. This was done so as not to obscure the point that a dynamic measurement is more representative than

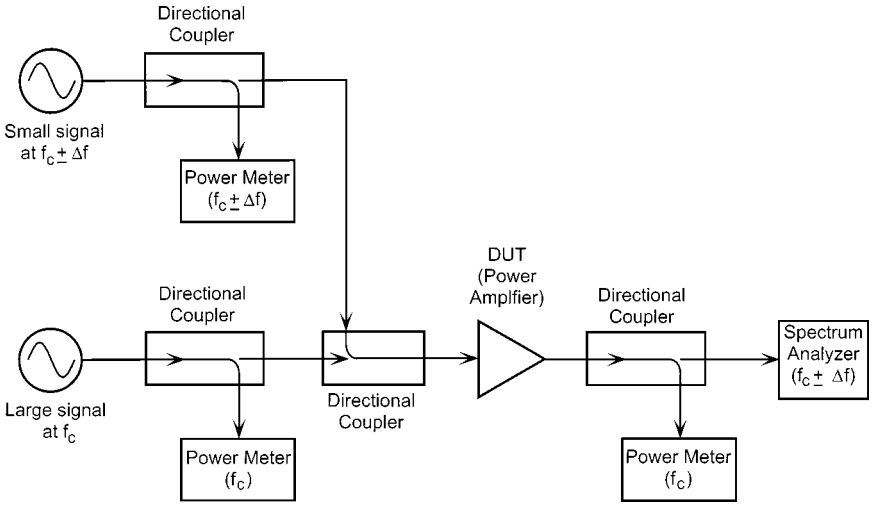

Fig. 2. Dynamic AM/AM, AM/PM test configuration.

a static measurement in characterizing the actual operation of a power amplifier in modulated signal contexts.

In order to deembed the various components of the proposed model from input/output measurements, it is necessary to calculate the output $y(t)$ for two special cases of its input $u(t)$: a small-signal two tone and a large-signal two tone. The two tone will consist of a large tone at the center frequency f_c and a small tone at some offset frequency

$$f_s =: f_\pm = f_c \pm \Delta f \tag{4}$$

where Δf is the magnitude of the frequency offset. More precisely,

$$u(t) = A\cos(\omega_c t + \theta_A) + a\cos(\omega_\pm t + \theta_a), \qquad A, a > 0 \tag{5}$$

where the phases θ_A and θ_a are arbitrary. The calculations for both types of two-tone inputs—i.e., with the small tone above or below the main carrier, designated as the high-side and low-side injection cases—will be done simultaneously. By convention, the upper (lower) signs in the following results will apply to the high-side (low-side) injection cases, respectively, unless otherwise stated.

Suppose the power amplifier is subjected to a small-signal two tone, as in (5), so that $A =: A_s$ and $a =: a_s$ are small enough for the gain and phase conversions to be given by

$$G(V_i, f_s - f_c) = G_s V_i \quad \phi(V_i, f_s - f_c) = \phi_s \tag{6}$$

where G_s and ϕ_s are constants for all f_s in the passband of the amplifier. It is clear that the output of the three-box model in Fig. 1 would consist of the same two tones as went in, modified in amplitude and phase as follows:

$$\begin{aligned} y(t) = {} & A_s G_s \big|H_1(f_c)\big|\big|H_2(f_c)\big| \\ & \times \cos\left[\omega_c t + \theta_{A_s} + \phi_s + \angle H_1(f_c) + \angle H_2(f_c)\right] \\ & + a_s G_s \big|H_1(f_\pm)\big|\big|H_2(f_\pm)\big| \\ & \times \cos\left[\omega_\pm t + \theta_{a_s} + \phi_s + \angle H_1(f_\pm) + \angle H_2(f_\pm)\right]. \end{aligned} \tag{7}$$

For the sake of notational simplicity, we let a_s and θ_{a_s} denote both of the two possibly different values of the offset-tone amplitudes and phases, respectively, for the two injection cases. However, we will assume that the carrier amplitude A_s and phase θ_{A_s} are identical for the two injection cases, respectively. The latter assumption will be used below for the large-signal two-tone input case.

From power meter and spectrum analyzer measurements made at the input and output of the power amplifier (see Fig. 2), the following ratios are calculated with the help of (7):

$$\begin{aligned} M^r_{i\pm} &:= \frac{\text{Input small-signal amplitude at } f_\pm}{\text{Input small-signal amplitude at } f_c} \\ &=: \frac{V^r_{i\pm}}{V^r_{ic}} \\ &= \frac{a_s}{A_s} \\ &=: \alpha_s \end{aligned} \tag{8a}$$

$$\begin{aligned} M^r_{o\pm} &:= \frac{\text{Output amplitude at } f_\pm}{\text{Output amplitude at } f_c} \\ &=: \frac{V^r_{o\pm}}{V^r_{oc}} \\ &= \alpha_s \frac{\big|H_1(f_\pm)\big|\big|H_2(f_\pm)\big|}{\big|H_1(f_c)\big|\big|H_2(f_c)\big|}. \end{aligned} \tag{8b}$$

The superscript 'r' in these quantities indicates that they are reference measurements performed under linear operation. Note from (8) that

$$\frac{M^r_{o\pm}}{M^r_{i\pm}} = \frac{\big|H_1(f_\pm)\big|\big|H_2(f_\pm)\big|}{\big|H_1(f_c)\big|\big|H_2(f_c)\big|}. \tag{9}$$

For the large-signal two-tone case, we let the tonal amplitudes be simply denoted by A and a, with the additional condition that $a \ll A$. Due to the distinct separation of frequencies in $u(t)$ [as seen from (5)] and linearity, it is clear that the output of the first filter $H_1(f) = |H_1(f)|e^{j\angle H_1(f)}$ will be given by

$$v(t) = B\cos(\omega_c t + \theta_B) + b_\pm \cos(\omega_\pm t + \theta_{b\pm}) \tag{10a}$$

where

$$\left.\begin{aligned} B &:= A\big|H_1(f_c)\big|, \quad b_\pm := a\big|H_1(f_\pm)\big| \\ \theta_B &:= \theta_A + \angle H_1(f_c), \quad \theta_{b\pm} := \theta_a + \angle H_1(f_\pm) \end{aligned}\right\}. \tag{10b}$$

From (10b), it will be convenient to define the ratio

$$\beta_{\pm} := \frac{b_{\pm}}{B} = \alpha \left| \frac{H_1(f_{\pm})}{H_1(f_c)} \right| \quad \alpha := \frac{a}{A}. \tag{11}$$

In view of (11), we will assume that the gain of the filter $H_1(f)$ is such that $\beta_{\pm} \ll 1$ as well. In parallel with [9], $v(t)$ must be expressed in terms of an AM and PM modulated carrier at the frequency f_c in order for the dynamic conversions to be applied. Using standard results from analytical signal theory [20], $v(t)$ can be written as

$$v(t) = V_i(t) \cos\left[\omega_c t + \theta_i(t)\right] \tag{12a}$$

where

$$\left.\begin{aligned} V_i(t) &= \sqrt{v_I^2(t) + v_Q^2(t)} \\ \theta_i(t) &= \tan^{-1}\left[\frac{v_Q(t)}{v_I(t)}\right] \end{aligned}\right\} \tag{12b}$$

and

$$\left.\begin{aligned} v_I(t) &= v(t)\cos(\omega_c t) + \hat{v}(t)\sin(\omega_c t) \\ v_Q(t) &= -v(t)\sin(\omega_c t) + \hat{v}(t)\cos(\omega_c t) \end{aligned}\right\}. \tag{12c}$$

$\hat{v}(t)$ is the Hilbert transform of $v(t)$ in (10a) given by

$$\hat{v}(t) = B\sin(\omega_c t + \theta_B) + b_{\pm}\sin(\omega_{\pm} t + \theta_{b\pm}). \tag{12d}$$

From (10a) and (12b)–(12d), one can show that the amplitude and phase modulations are given exactly by

$$V_i(t) = B\Big[1 + \beta_{\pm}^2 + 2\beta_{\pm}\cos(\pm\Delta\omega t + \theta_{bB}^{\pm})\Big]^{1/2} \tag{13a}$$

where

$$\theta_{bB}^{\pm} := \theta_{b\pm} - \theta_B \tag{13b}$$

and

$$\theta_i(t) = \tan^{-1}\left[\frac{\sin\theta_B + \beta_{\pm}\sin(\pm\Delta\omega t + \theta_{b\pm})}{\cos\theta_B + \beta_{\pm}\cos(\pm\Delta\omega t + \theta_{b\pm})}\right] \tag{13c}$$

respectively. To order $\beta_{\pm}$, these expressions can be expanded in a Maclaurin series as follows:

$$V_i(t) = B\left[1 + \beta_{\pm}\cos(\pm\Delta\omega t + \theta_{bB}^{\pm})\right] + \mathcal{O}(\beta_{\pm}^2) \tag{14a}$$

$$\theta_i(t) = \theta_B + \beta_{\pm}\sin\left(\pm\Delta\omega t + \theta_{bB}^{\pm}\right) + \mathcal{O}(\beta_{\pm}^2). \tag{14b}$$

These expressions will be useful below when a similar expansion is done for the output $w(t)$ of the memoryless nonlinearity.

Applying the two-tone dynamic conversions to the signal in (12a) yields

$$w(t) = G\big[V_i(t), \pm\Delta f\big]\cos\Big\{\omega_c t + \theta_i(t) + \phi\big[V_i(t), \pm\Delta f\big]\Big\} \tag{15}$$

where $V_i(t)$ is as in (13a) or (14a), and $\theta_i(t)$ is as in (13c) or (14b). Finally, for the general case, the output of the three-box model would be

$$y(t) = w(t) \circledast h_2(t) = \int_{0^-}^{t} h_2(\tau) w(t-\tau)\, d\tau \tag{16}$$

where $h_2(t)$ is the impulse response corresponding to the filter $H_2(f)$ [i.e., $h_2(t) = \int_{-\infty}^{\infty} H_2(f) e^{j2\pi f t} df$]. In order to develop the two-tone dynamic method, it is necessary to expand $w(t)$ in (15) about $\beta_{\pm} = 0$, keeping terms only up to order $\beta_{\pm}$, as follows:

$$w(t) = w(t)\big|_{\beta_{\pm}=0} + \left.\frac{\partial w(t)}{\partial \beta_{\pm}}\right|_{\beta_{\pm}=0} \beta_{\pm} + \mathcal{O}(\beta_{\pm}^2). \tag{17}$$

Denoting by $w^{\text{hs}}(t)$ and $w^{\text{ls}}(t)$ the expansion in (17) for the case of high- and low-side injections, respectively, it follows from (14) and (15) and several trigonometric identity manipulations that

$$\begin{aligned} w^{\text{hs}}(t) = {} & G(B,\Delta f)\cos\left[\omega_c t + \theta_B + \phi(B,\Delta f)\right] \\ & + \beta_+ G(B,\Delta f)\Big\{S_+^{\text{hs}}\cos\left(\omega_+ t + \phi_+^{\text{hs}}\right) \\ & - S_-^{\text{hs}}\cos(\omega_- t + \phi_-^{\text{hs}})\Big\} + \mathcal{O}(\beta_+^2) \end{aligned} \tag{18a}$$

where

$$\begin{aligned} S_{\pm}^{\text{hs}} &= S_{\pm}^{\text{hs}}(B,\Delta f) \\ &= \frac{1}{2}\left\{\left[1 \pm \frac{BG'(B,\Delta f)}{G(B,\Delta f)}\right]^2 + [B\phi'(B,\Delta f)]^2\right\}^{1/2} \end{aligned} \tag{18b}$$

$$\phi_+^{\text{hs}} = \phi_+^{\text{hs}}(B,\Delta f) = \theta_{b+} + \theta_+^{\text{hs}} \tag{18c}$$

$$\phi_-^{\text{hs}} = \phi_-^{\text{hs}}(B,\Delta f) = 2\theta_B - \theta_{b+} + \theta_-^{\text{hs}} \tag{18d}$$

$$\begin{aligned} \theta_{\pm}^{\text{hs}} &= \theta_{\pm}^{\text{hs}}(B,\Delta f) \\ &= \phi(B,\Delta f) \pm \tan^{-1}\left[\frac{B\phi'(B,\Delta f)}{1 \pm \dfrac{BG'(B,\Delta f)}{G(B,\Delta f)}}\right] \end{aligned} \tag{18e}$$

and

$$\begin{aligned} w^{\text{ls}}(t) = {} & G(B,-\Delta f)\cos\left[\omega_c t + \theta_B + \phi(B,-\Delta f)\right] \\ & + \beta_- G(B,-\Delta f)\big\{S_-^{\text{ls}}\cos(\omega_- t + \phi_-^{\text{ls}}) \\ & - S_+^{\text{ls}}\cos(\omega_+ t + \phi_+^{\text{ls}})\big\} + \mathcal{O}\left(\beta_-^2\right) \end{aligned} \tag{19a}$$

where

$$S_{\pm}^{\text{ls}} = S_{\pm}^{\text{ls}}(B,\Delta f) = S_{\mp}^{\text{hs}}(B,\Delta f \to -\Delta f) \tag{19b}$$

$$\phi_{\pm}^{\text{ls}} = \phi_{\pm}^{\text{ls}}(B,\Delta f) = \phi_{\mp}^{\text{hs}}(B,\theta_{b+} \to \theta_{b-}, \Delta f \to -\Delta f) \tag{19c}$$

and $\tan^{-1}(n/d)$ falls in the quadrant dictated by the location of the ordered pair (d,n).

Passing the responses $w^{\text{hs}}(t)$ and $w^{\text{ls}}(t)$ through the second filter $H_2(f)$ in the three-box model leads to the final outputs

$$\begin{aligned} & y^{\text{hs}}(t) \\ & = |H_2(f_c)|G(B,\Delta f)\cos\left[\omega_c t + \theta_B + \phi(B,\Delta f) + \angle H_2(f_c)\right] \\ & \quad + \beta_+ G(B,\Delta f)\Big\{|H_2(f_+)|S_+^{\text{hs}}\cos\left[\omega_+ t + \phi_+^{\text{hs}} + \angle H_2(f_+)\right] \\ & \quad - |H_2(f_-)|S_-^{\text{hs}}\cos\left[\omega_- t + \phi_-^{\text{hs}} + \angle H_2(f_-)\right]\Big\} + \mathcal{O}\left(\beta_+^2\right) \end{aligned} \tag{20}$$

and

$$\begin{aligned} y^{\mathrm{ls}}(t) &= |H_2(f_c)|G(B,-\Delta f)\cos\left[\omega_c t+\theta_B+\phi(B,-\Delta f)\right. \\ &\quad \left.+\angle H_2(f_c)\right]+\beta_- G(B,-\Delta f) \\ &\quad \times\Big\{|H_2(f_-)|S_-^{\mathrm{ls}}\cos\left[\omega_- t+\phi_-^{\mathrm{ls}}+\angle H_2(f_-)\right] \\ &\quad -|H_2(f_+)|S_+^{\mathrm{ls}}\cos\left[\omega_+ t+\phi_+^{\mathrm{ls}}+\angle H_2(f_+)\right]\Big\}+\mathcal{O}(\beta_-^2). \end{aligned} \tag{21}$$

Proceeding in a manner similar to the small-signal case, we calculate from (11), (20), and (21) the following measurement ratios:

$$\begin{aligned} M_{i\pm} &:= \frac{\text{Input large-signal amplitude at}\, f_\pm}{\text{Input large-signal amplitude at}\, f_c} \\ &=: \frac{V_{i\pm}}{V_{ic}} \\ &= \alpha \end{aligned} \tag{22a}$$

$$\begin{aligned} M_{o\pm}^{\mathrm{hs}} &:= \frac{\text{High-side output amplitude at}\, f_\pm}{\text{High-side output amplitude at}\, f_c} \\ &=: \frac{V_{o\pm}^{\mathrm{hs}}}{V_{oc}^{\mathrm{hs}}} \\ &= \pm\frac{|H_1(f_+)||H_2(f_\pm)|}{|H_1(f_c)||H_2(f_c)|}\alpha S_\pm^{\mathrm{hs}} \end{aligned} \tag{22b}$$

$$\begin{aligned} M_{o\pm}^{\mathrm{ls}} &:= \frac{\text{Low-side output amplitude at}\, f_\pm}{\text{Low-side output amplitude at}\, f_c} \\ &=: \frac{V_{o\pm}^{\mathrm{ls}}}{V_{oc}^{\mathrm{ls}}} \\ &= \mp\frac{|H_1(f_-)||H_2(f_\pm)|}{|H_1(f_c)||H_2(f_c)|}\alpha S_\pm^{\mathrm{ls}}. \end{aligned} \tag{22c}$$

Since the input large-signal amplitude A remains identical for the two injection cases, it follows that $V_{oc}^{hs}=V_{oc}^{\mathrm{ls}}$. In these measurements, if the ratio $\beta_\pm$ is -30 dB, then the error in our expansions for $y^{\mathrm{hs}}(t)$ and $y^{\mathrm{ls}}(t)$ is approximately 3%. If we accepted a ratio of -24 dB, then the error would be approximately 6%.

One of the basic components of the model to deembed are the dynamic gain and phase conversions. From (18b) and (19b), we see that the quantities $S_\pm^{\mathrm{hs}}$ and $S_\pm^{\mathrm{ls}}$ contain the necessary elements to construct a good approximation to the desired conversions. Using the measurement ratios in (9) and (22), we can solve for $S_\pm^{\mathrm{hs}}$ and $S_\pm^{\mathrm{ls}}$ to arrive at

$$\left.\begin{aligned} S_+^{\mathrm{hs}} &= \left(\frac{M_{o+}^{\mathrm{hs}}}{M_{i+}}\right)\left(\frac{M_{i+}^r}{M_{o+}^r}\right) \\ S_-^{\mathrm{hs}} &= -\left(\frac{M_{o-}^{\mathrm{hs}}}{M_{i-}}\right)\left(\frac{M_{i+}^r}{M_{o+}^r}\right)\left(\frac{|H_2(f_+)|}{|H_2(f_-)|}\right) \end{aligned}\right\} \tag{23a}$$

and

$$\left.\begin{aligned} S_+^{\mathrm{ls}} &= S_-^{\mathrm{hs}}(\mathrm{hs}\to\mathrm{ls},\mathrm{sub}-\to\mathrm{sub}+) \\ S_-^{\mathrm{ls}} &= S_+^{\mathrm{hs}}(\mathrm{hs}\to\mathrm{ls},\mathrm{sub}+\to\mathrm{sub}-) \end{aligned}\right\}. \tag{23b}$$

With the results of this two-tone analysis, the components of the three-box model in Fig. 1 can be derived, as will be described in Section II-B.

B. Three-Box Model Identification

The determination of the components of the newly proposed dynamic three-box model is a generalization of that already done for the static case of the model. It is a two-part process, the first part involving the determination of the two linear filter responses, while the second part concerns the deembedment of the dynamic amplitude and phase conversions. As will be seen from the treatment below, the components of the model are not uniquely determined from the small-/large-signal measurements just presented. As a consequence, there are many possible versions of the model that can be proposed, each one distinguished by the particular choice of additional constraints imposed on the model components. For simplicity, only a few representative versions of the model will be presented here.

1) Filter Response Determination: The first additional constraint to consider occurs in the small-signal regime of operation, involving the apportionment of the gain and phase shift of the power amplifier between the two linear filters and the two dynamic conversion curves [see (7)]. By convention, there is only one set of dynamic conversion curves to be used in any given manifestation of this model. These curves are always referenced to the center-band frequency f_c, are chosen for some fixed and convenient offset frequency Δf, and are based on either high- or low-side injections. As such, it follows that the two linear filters will bestow frequency dependence upon these two curves through the actions of their gains and phases. In the course of the model identification, however, it will be necessary for both f_c and Δf to vary in order to cover the passband of the power amplifier. There are two representative approaches that can be proposed for the model's small-signal response decomposition. The first approach would impose the condition that the two dynamic conversion curves have unity gain ($G_s=1$) and zero phase shift ($\phi_s=0$) in their small-signal regimes, respectively, for all Δf and f_c. This allows the two linear filters to exactly contain the small-signal behavior of the power amplifier. In the second approach, the small-signal gain and phase of the dynamic conversion curves are not set to a particular pair of values, but are still constrained to be constant across the passband of the power amplifier, while the two linear filters are restricted at the center frequency f_c to be given by

$$H_1(f_c)\equiv\frac{1}{A_{\max}}\quad H_2(f_c)\equiv 1. \tag{24}$$

Here, $A_{\max}$ designates the value of the input carrier amplitude A to the power amplifier that maximizes its output carrier amplitude for the two-tone offset and injection type to be used in the final model. In this case, the two filters have zero phase at the center frequency, and the small-signal constants G_s and ϕ_s in (6) can be determined from direct input/output measurements. Using (24) in (7), it follows that the small-signal carrier gain and phase of the memoryless nonlinearity at f_c (and for all other frequencies and offsets) is given by

$$G_s=\frac{A_{\max}V_{oc}^r}{A_s}\quad \phi_s=\phi_{oc}^r-\theta_{A_s} \tag{25}$$

where the input carrier amplitude A_s is chosen small enough so that the power amplifier is operating in its linear regime, and $V_{oc}^r(\phi_{oc}^r)$ is the small-signal carrier amplitude (phase shift) at f_c. Note that if a small-signal VNA sweep of the power amplifier

is also made [denoted by $M_{ss}(f)$], then for the first approach it follows from (7)—with $a_s = 0$ and $f_c = f$ varying across the band—that

$$\left.\begin{aligned} |M_{ss}(f)| &= |H_1(f)||H_2(f)| \\ \angle M_{ss}(f) &= \angle H_1(f) + \angle H_2(f) \end{aligned}\right\} \tag{26a}$$

while for the second approach

$$\left.\begin{aligned} |M_{ss}(f)| &= G_s|H_1(f)||H_2(f)| \\ \angle M_{ss}(f) &= \angle H_1(f) + \angle H_2(f) + \phi_s \end{aligned}\right\} \tag{26b}$$

where G_s and ϕ_s are as shown in (25).

Despite the imposition of the above conditions, it can be seen from (7), (23) and (26) that the two linear filter responses are still not determined uniquely. To pin down these responses, several possible additional conditions can be imposed that separately determine the gain and then phase responses of the two filters. For the gain responses, there are two possible ways of obtaining $|H_2(f)|$ that can be proposed, with $|H_1(f)|$ then following immediately from (26). The first way to obtain the gain response of $H_2(f)$ is based on (23). In particular, $|H_2(f)|$ is taken to be such that

$$S_+^{\text{ls}} = S_-^{\text{hs}} =: S_o. \tag{27}$$

It then follows from (23a), (23b), and (27) that

$$S_o = \left[\left(\frac{M_{o-}^{\text{hs}}}{M_{i-}}\right)\left(\frac{M_{i+}^r}{M_{o+}^r}\right)\left(\frac{M_{o+}^{\text{ls}}}{M_{i+}}\right)\left(\frac{M_{i-}^r}{M_{o-}^r}\right)\right]^{1/2} \tag{28}$$

and

$$\left|\frac{H_2(f_+)}{H_2(f_-)}\right| = \left[\left(\frac{M_{i-}}{M_{o-}^{\text{hs}}}\right)\left(\frac{M_{o+}^r}{M_{i+}^r}\right)\left(\frac{M_{o+}^{\text{ls}}}{M_{i+}}\right)\left(\frac{M_{i-}^r}{M_{o-}^r}\right)\right]^{1/2}. \tag{29}$$

Observe that the expression in (29) provides the ratio in gain of the filter $H_2(f)$ between the sidebands. By varying the center frequency f_c entering the power amplifier, and fixing the frequency location of one of the sidebands by the appropriate choice of the frequency offset Δf, the actual gain of $H_2(f)$ can be calculated to within a constant that is equal to the absolute gain of $H_2(f)$ at the fixed sideband frequency. In particular, if $|H_2(f)|$ is to be determined at N frequency points, one could fix the lower sideband at the lower band-edge frequency f_-, with some initial choice of Δf that is equal to half of the desired frequency resolution for $|H_2(f)|$, and with an absolute gain of $G_1 := |H_2(f_-)|$. Calculating the quantity on the right-hand side of (29) would then give $|H_2(f_+)|$ to within the constant G_1. Moving f_c to where f_+ was and repeating the necessary measurements and calculations with Δf replaced by $2\Delta f$ will result in $|H_2(f_- + 4\Delta f)|$ modulo G_1. One can then continue in this manner to arrive at $|H_2(f_- + 2k\Delta f)| \operatorname{modulo} G_1, k = 1, \ldots, N$. Note that each time the center frequency is moved, the measurement of the eight ratios in the right-hand side of (29) must be done, although this can be easily automated to make it a relatively quick procedure. One may not want to use the lower frequency point f_- as the reference since the band edge often has a lower signal level and a lower SNR than other frequencies. To overcome this problem, choose f_- to be midband and proceed as outlined above. Then fix the upper sideband frequency f_+ to be equal to f_- and proceed to obtain the lower part of the band in a complementary manner. In this way, $|H_2(f)|$ will be obtained relative to the midband frequency gain. Finally, in the case that (24) is imposed, the obtained gain of $H_2(f)$ can be shifted to arrive at a unique response solution.

The second simpler and more preferable means of determining $|H_2(f)|$ involves the imposition of an additional normalization condition on the particular dynamic amplitude conversion curve chosen for the model as a function of its center frequency f_c. In essence, this condition will focus on maintaining the constancy of the maximum of this curve with respect to f_c, imparting all of its frequency dependence to $|H_2(f)|$. This method is also more physical in its interpretation and will automatically lead to gain responses that satisfy condition (24). The specific procedure is as follows. First choose a set of frequencies $f_k, k = \ldots, -1, 0, 1, \ldots$ that covers the power-amplifier passband, includes the center-band frequency f_c (with f_0 defined to be f_c), and are uniformly spaced by the desired frequency resolution for the resulting gain response. Next, choose the desired two-tone separation Δf and injection type that will be used in the model's center box. Letting the carrier frequency take on the value of f_k, apply a two tone to the power amplifier with the usual condition that the amplitude ratio α in (11) is much less than one. Vary the amplitude A of the input carrier until the output amplitude at f_k reaches its maximum $C_{\max} = C_{\max}(f_k)$. The gain response of $H_2(f)$ is then given by

$$|H_2(f_k)| = \frac{C_{\max}(f_k)}{C_{\max}(f_c)}, \qquad k = \ldots, -1, 0, 1, \ldots. \tag{30}$$

It should be emphasized here that if a different two-tone separation or injection type is to be used in the model, this procedure must be repeated since $|H_2(f)|$ will necessarily change.

In the same manner as for the gain, the phase of $H_2(f)$ can be obtained in two different ways, with the phase of $H_1(f)$ again immediately following from (26) (directly for the first method and implicitly for the second). In this case, the first simpler way of obtaining $\angle H_2(f)$ is essentially artificial, while the second more complicated approach provides a rigorous result. The first approach is analogous to the second one used to obtain the gain response of $H_2(f)$ in that the same set of two-tone measurements are made as described above. Again, the amplitude A of the input carrier is varied until the output amplitude at f_k reaches its maximum, but the total carrier phase change $\Phi_{\max} = \Phi_{\max}(f_k)$ with this input is noted instead. The phase response of $H_2(f)$ is then given by

$$\angle H_2(f_k) = \Phi_{\max}(f_k) - \Phi_{\max}(f_c), \qquad k = \ldots, -1, 0, 1, \ldots. \tag{31}$$

Note from (31) that $\angle H_2(f_0) = 0$, thus satisfying condition (24). This approach can be considered arbitrary since it is one of an infinite number of ways of distributing the actual carrier frequency dependence of the dynamic AM/PM conversion between the phases of the two linear filters. This is in contrast to what occurs for the dynamic AM/AM conversion, where there is a clear and unique distribution of the carrier frequency dependence between the two filters. In fact, it can be seen from above that $|H_2(f)|$ takes care of the output variations of this conversion, while it is straightforward to see that $|H_1(f)|$ actually takes

care of the input variation of this conversion. Indeed, an alternative way of obtaining $|H_1(f)|$ is to take it to be given by

$$|H_1(f_k)| = \frac{1}{A_{\max}(f_k)}, \qquad k = \ldots, -1, 0, 1, \ldots \tag{32}$$

where $A_{\max}(f_k)$ represents the input carrier amplitude that gives the maximum output carrier amplitude $C_{\max}(f_k)$. Again, this result is consistent with condition (24) since $A_{\max}(f_0) = A_{\max}$ defined there. Of course, the result in (32) must be consistent with that obtained from small-signal VNA measurements via (26).

The second method of calculating $\angle H_2(f)$ actually encompasses the rigorous determination of both filter phases, and requires that the procedure in the following subsection be applied first in order to arrive at the necessary dynamic AM/PM conversions $\phi(\hat{V}_{ic}, \Delta f)$ for the appropriate offset amplitude Δf and carrier frequencies. It suffices to mention here that this latter procedure only requires the *a priori* knowledge of the gain responses of the two filters, and these would have already been obtained as outlined above. The basic procedure is as follows, which begins at the center-band frequency f_c and then walks across the passband, using low-side injection to the right of f_c and high-side injection to the left of f_c. Again, a filter resolution Δf is chosen for the phase responses, and both small- and large-signal measurements are made at the first three frequencies

$$f_{0\pm} := f_c \pm \Delta f. \tag{33}$$

For the small-signal VNA measurements made with the two tone in (5), the following equations would be obtained from (7), relating the measured phase shifts $\Delta\psi_c, \Delta\psi_{0\pm}$ between the output phases $\psi_c, \psi_{0\pm}$ and the input arbitrary phases $\theta_{A_s}, \theta_{a_s}$, respectively, at the three frequencies $f_{0\pm}$:

$$\Delta\psi_c = \psi_c - \theta_{A_s} = \phi_s + \angle H_1(f_c) + \angle H_2(f_c) \tag{34a}$$

$$\Delta\psi_{0\pm} = \psi_{0\pm} - \theta_{a_s} = \phi_s + \angle H_1(f_{0\pm}) + \angle H_2(f_{0\pm}) \tag{34b}$$

where, again, the small-signal phase conversion ϕ_s is taken to be constant for all frequencies in the amplifier passband. Moving into the large-signal regime, the input carrier amplitude $A_{\pm}^{\text{sat}}$ that provides the maximum output carrier amplitude for both high- and low-side injections would be noted (they could be different values), providing the values

$$B_{\pm}^{\text{sat}} = A_{\pm}^{\text{sat}} \big| H_1(f_c) \big| \tag{35}$$

for the input to the dynamic conversion box using (10b) and the previously calculated gain response $|H_1(f)|$. Using these two tones as inputs, time-domain measurements would be made and Fourier analysis would be used to arrive at the phases (up to an arbitrary constant) at the three frequencies. If high carrier frequencies are involved, then accurate time-domain measurements can be obtained using a previously developed baseband technique [18], [19]. Using (10b) and (18)–(21), six additional relations would arise, the three for the high-side injection case given by

$$\Psi_c^{\text{hs}} = \theta_A + \phi_{0+}^{\text{sat}} + \angle H_1(f_c) + \angle H_2(f_c) \tag{36a}$$

$$\Psi_{0+}^{\text{hs}} = \theta_a + \phi_{0+}^{\text{sat}} + \tan^{-1}\left(B_+^{\text{sat}} \rho_{0+}^{\text{sat}}\right) + \angle H_1(f_{0+}) + \angle H_2(f_{0+}) \tag{36b}$$

$$\Psi_{0-}^{\text{hs}} = 2\theta_A - \theta_a + \phi_{0+}^{\text{sat}} - \tan^{-1}(B_+^{\text{sat}} \rho_{0+}^{\text{sat}}) + 2\angle H_1(f_c) - \angle H_1(f_{0+}) + \angle H_2(f_{0-}) \tag{36c}$$

where

$$\phi_{0+}^{\text{sat}} := \phi(B_+^{\text{sat}}, \Delta f) \quad \rho_{0+}^{\text{sat}} := \phi'(B_+^{\text{sat}}, \Delta f) \tag{36d}$$

involving the previously determined dynamic AM/PM conversion $\phi(\hat{V}_{ic}, \Delta f)$. The expressions for the low-side injection case would be entirely similar with subscript $+(-)$ replaced by subscript $-(+)$, superscript hs replaced by superscript ls, and Δf replaced with $-\Delta f$ in (36). Using basic Gaussian elimination, it turns out that the above nine conditions reduce to four independent ones on the six unknowns $\angle H_i(f_c), \angle H_i(f_{0\pm}), i = 1, 2$, hence, allowing for two free variables that must be chosen in value. Suppose the four basic variables are taken to be $\angle H_1(f_{0\pm}), \angle H_1(f_c)$, and $\angle H_2(f_{0-})$, and let the free variables be $\angle H_2(f_c)$ and $\angle H_2(f_{0+})$, with values set to

$$\angle H_2(f_c) = 0 \quad \angle H_2(f_{0+}) = -\tau_{sc}\Delta f \tag{37}$$

where τ_{sc} is the delay through the power amplifier at center band under small-signal excitation. Finally, suppose that

$$\phi_s = \Delta\psi_c \tag{38}$$

i.e., all the center-band small-signal phase shift occurs in the model's nonlinear box, as done in (25). It can then be shown that the solution to the four remaining independent equations is given by

$$\angle H_1(f_{0-}) = \Delta\psi_{0-} - \Delta\psi_{0+} - \Psi_{0+}^{\text{hs}} + 2\theta_A - \theta_a + \phi_{0+}^{\text{sat}} - \tan^{-1}(B_-^{\text{sat}} \rho_{0+}^{\text{sat}}) - \tau_{sc}\Delta f \tag{39a}$$

$$\angle H_1(f_c) = 0 \tag{39b}$$

$$\angle H_1(f_{0+}) = \Delta\psi_{0+} - \Delta\psi_c + \tau_{sc}\Delta f \tag{39c}$$

$$\angle H_2(f_{0-}) = \Delta\psi_{0-} - \Delta\psi_c - \angle H_1(f_{0-}). \tag{39d}$$

Note that the zero phases for the two filters at f_c is consistent with (24).

To determine $\angle H_i(f), i = 1, 2$ across the amplifier passband, a Δf stepping process is taken to the right and left of f_c, keeping the spacing between the two tones at Δf. Let the frequency of the large carrier be denoted by

$$f_n := f_c + n\Delta f, \qquad n = \ldots, -1, 0, 1, \ldots \tag{40a}$$

with $f_0 := f_c$. Let the sideband frequencies for the two injection types be denoted by

$$f_{n\pm} := f_n \pm \Delta f, \qquad n = \ldots, -1, 0, 1, \ldots. \tag{40b}$$

It can then be shown, in general, that for $n = k, k = 1, 2, \ldots$

$$f_k = f_{(k-1)+} \quad f_{k-} = f_{k-1} \tag{41a}$$

while for $n = -k, k = 1, 2, \ldots$

$$f_{-k+} = f_{-k+1} \quad f_{-k} = f_{(-k+1)-}. \tag{41b}$$

In addition, for each $n = \pm k, k = 2, \ldots$, there are only two more unknowns to be determined, namely, $\angle H_i(f_{k+}), i = 1, 2$ for $n = k$ and $\angle H_i(f_{-k-}), i = 1, 2$ for $n = -k$. This is because results from the previous value of n apply to the current value through the relations in (41). The two additional independent equations needed to determine these unknowns come from a small-signal VNA measurement at $f_{\pm k\pm}$ for $n = \pm k$, as well as a low-side (high-side) two-tone injection at $f_k(f_{-k})$ for which

the phase for the opposite sideband at $f_{k+}(f_{-k-})$ is determined. Explicitly, these equations are

$$\Delta\psi_{k+} = \phi_s + \angle H_1(f_{k+}) + \angle H_2(f_{k+}) \quad (n=k) \tag{42a}$$

$$\Delta\psi_{-k-} = \phi_s + \angle H_1(f_{-k-}) + \angle H_2(f_{-k-}) \quad (n=-k) \tag{42b}$$

for the small-signal VNA measurements, while for the large-signal measurements they are

$$\left.\begin{aligned}\Psi^{\rm ls}_{k+} \quad &= 2\theta_A - \theta_a + \phi^{\rm sat}_{k-} - \tan^{-1}\left(B^{\rm sat}_{-}\rho^{\rm sat}_{k-}\right)\\ &\quad +2\angle H_1\left(f_{(k-1)+}\right) - \angle H_1(f_{k-1}) + \angle H_2(f_{k+})\end{aligned}\right\} \tag{43a}$$

for $n = k$ and

$$\begin{aligned}\Psi^{\rm hs}_{-k-} = {} & 2\theta_A - \theta_a + \phi^{\rm sat}_{-k+} - \tan^{-1}\left(B^{\rm sat}_{+}\rho^{\rm sat}_{-k+}\right)\\ & +2\angle H_1\left(f_{(-k+1)-}\right) - \angle H_1(f_{-k+1}) + \angle H_2(f_{-k-})\end{aligned} \tag{43b}$$

for $n = -k$, which are generalizations of (36c) and its low-side complement, and we have used and (41). Observe that the quantities $\angle H_1(f_{(k-1)+}), \angle H_1(f_{k-1}), \angle H_1(f_{-k+1})$, and $\angle H_1(f_{(-k+1)-})$ are already known from the previous measurements taken with $n = \pm(k-1)$. The solutions of (42)–(43) and for the special case (38) are given by

$$\begin{aligned}\angle H_1(f_{k+}) = {} & \Delta\psi_{k+} - \Delta\psi_c - \Psi^{\rm ls}_{k+} + 2\theta_A\\ & - \theta_a + \phi^{\rm sat}_{k-} - \tan^{-1}\left(B^{\rm sat}_{-}\rho^{\rm sat}_{k-}\right)\\ & + 2\angle H_1\left(f_{(k-1)+}\right) - \angle H_1(f_{k-1})\end{aligned} \tag{44a}$$

and

$$\begin{aligned}\angle H_2(f_{k+}) = {} & \Psi^{\rm ls}_{k+} - 2\theta_A + \theta_a - \phi^{\rm sat}_{k-} + \tan^{-1}\left(B^{\rm sat}_{-}\rho^{\rm sat}_{k-}\right)\\ & -2\angle H_1(f_{(k-1)+}) + \angle H_1(f_{k-1})\end{aligned} \tag{44b}$$

for $n = k$, and

$$\begin{aligned}\angle H_1(f_{-k-}) = {} & \Delta\psi_{-k-} - \Delta\psi_c - \Psi^{\rm hs}_{-k-} + 2\theta_A - \theta_a + \phi^{\rm sat}_{-k+}\\ & - \tan^{-1}\left(B^{\rm sat}_{+}\rho^{\rm sat}_{-k+}\right) + 2\angle H_1\left(f_{(-k+1)-}\right)\\ & - \angle H_1\left(f_{-k+1}\right)\end{aligned} \tag{45a}$$

and

$$\begin{aligned}\angle H_2(f_{-k-}) = {} & \Psi^{\rm hs}_{-k-} - 2\theta_A + \theta_a - \phi^{\rm sat}_{-k+}\\ & + \tan^{-1}\left(B^{\rm sat}_{+}\rho^{\rm sat}_{-k+}\right) - 2\angle H_1\left(f_{(-k+1)-}\right)\\ & + \angle H_1\left(f_{-k+1}\right)\end{aligned} \tag{45b}$$

for $n = -k$. To recap, the following remarks are in order concerning the phase response solutions in (39), (44), and (45).

1) The phase shifts $\Delta\psi_{\pm k\pm}, k = 0, 1, \ldots$, and $\Delta\psi_c$ are directly measured by a VNA.
2) The time delay τ_{sc} is also a measured quantity.
3) The phase shifts $\Psi^{\rm ls,hs}_{\pm k\pm}, k = 0, 1, \ldots$ are obtained from a Fourier transform of a measured time-domain signal at the output of the power amplifier.
4) The phases θ_A and θ_a are arbitrary so that all the phases are known only up to an indeterminate constant.
5) The phase shifts $\phi^{\rm sat}_{\pm k\pm}, k = 0, 1, \ldots$ are obtained from the derived dynamic AM/PM conversions referenced to $f_{\pm k}$ in (40a) with offsets $\pm\Delta f$. The procedure for this derivation from spectrum analyzer measurements is the subject of Section II-B.2. The same comments hold for the slopes

$$\rho^{\rm sat}_{\pm k\pm} = \frac{d}{d\hat{V}_{ic}}\,\phi_{\pm k}\left(\hat{V}_{ic}, \pm\Delta f\right)\Big|_{\hat{V}_{ic}=B^{\rm sat}_{\pm}}. \tag{46}$$

6) The amplitudes $B^{\rm sat}_{\pm}$ are given by

$$B^{\rm sat}_{\pm} = A^{\rm sat}_{\pm}\left|H_1(f_n)\right| \tag{47}$$

which will vary with n and assume that the gain response $|H_1(f)|$ has already been obtained.

2) Dynamic Conversion Determination: The second part of the deembedment procedure is to obtain—using the sideband amplitude quantities $S^{\rm hs,ls}_{\pm}$ derived above from measurements—expressions for the dynamic AM/AM and AM/PM conversions and their derivatives at $\beta_{\pm} = 0$, thereby relating the input carrier amplitudes and phases to the output carrier amplitudes and phases for the memoryless nonlinearity. We will present a detailed discussion only for the high-side injection case, giving only the results for the complementary low-side injection case. Note from (18b) and the analogous voltage definitions in (8) and (22) applied to the memoryless nonlinearity in the three-box model (denoted with a "^" over the voltage variable) that

$$\begin{aligned}\left(S^{\rm hs}_{+}\right)^2 - \left(S^{\rm hs}_{-}\right)^2 &= \left[S^{\rm hs}_{+}\left(\hat{V}_{ic}, \Delta f\right)\right]^2 - \left[S^{\rm hs}_{-}\left(\hat{V}_{ic}, \Delta f\right)\right]^2\\ &= \frac{BG'(B,\Delta f)}{G(B,\Delta f)}\\ &= \frac{\hat{V}_{ic}}{\hat{V}^{\rm hs}_{oc}}\cdot\frac{\partial G(V_i,\Delta f)}{\partial V_i}\bigg|_{\beta_+\to 0}.\end{aligned} \tag{48}$$

Observe from (14a) that $V_i = \hat{V}_{ic}$ at $\beta_+ = 0$ and, hence, the functional dependence of $G(V_i, \Delta f)$ on V_i would be identical to that of $G(\hat{V}_{ic}, \Delta f)$ on $\hat{V}_{ic}$. Thus, their derivatives with respect to V_i and $\hat{V}_{ic}$, respectively, would also be functionally identical. Assuming that the partial derivatives of $G(V_i, \Delta f)$ are continuous with respect to V_i, and since V_i is smooth with respect to β_+, it follows that

$$\frac{\partial G(V_i,\Delta f)}{\partial V_i}\bigg|_{\beta_+\to 0} = \frac{\partial G\left(\hat{V}_{ic},\Delta f\right)}{\partial \hat{V}_{ic}} = \frac{d\hat{V}^{\rm hs}_{oc}}{d\hat{V}_{ic}} \tag{49}$$

for a fixed value of Δf. With (49) in (48), it follows that

$$\left(S^{\rm hs}_{+}\right)^2 - \left(S^{\rm hs}_{-}\right)^2 = \frac{\hat{V}_{ic}}{\hat{V}^{\rm hs}_{oc}}\cdot\frac{d\hat{V}^{\rm hs}_{oc}}{d\hat{V}_{ic}}. \tag{50}$$

Since it is standard to report AM/AM values in decibels/decibel, it will be necessary to convert the right-hand side of (50) to a logarithmic form. Observe that for a voltage V

$$dV = \frac{\ln 10}{20} V\, dV \text{ dB}. \tag{51}$$

Using (51) in (50), the dynamic carrier AM/AM is given by

$$\left.\begin{aligned}\frac{d\hat{V}^{\rm hs}_{oc}(\text{dB})}{d\hat{V}_{ic}(\text{dB})} &= \left(\tilde{S}^{\rm hs}_{+}\right)^2 - \left(\tilde{S}^{\rm hs}_{-}\right)^2\\ \tilde{S}^{\rm hs}_{\pm} &:= S^{\rm hs}_{\pm}\left(\hat{V}_{ic} = 10^{\hat{V}_{ic}(\text{dB})/20}, \Delta f\right)\end{aligned}\right\} \tag{52a}$$

and, similarly, for the low-side injection case by

$$\left.\begin{aligned}\frac{d\hat{V}_{oc}^{\rm ls}(\rm dB)}{d\hat{V}_{ic}(\rm dB)} &= \left(\tilde{S}_{-}^{\rm ls}\right)^2 - \left(\tilde{S}_{+}^{\rm ls}\right)^2 \\ \tilde{S}_{\pm}^{\rm ls} &:= S_{\pm}^{\rm ls}\left(\hat{V}_{ic} = 10^{\hat{V}_{ic}(\rm dB)/20}, \Delta f\right)\end{aligned}\right\}. \tag{52b}$$

Note that the right-hand sides in (52a) and (52b) are unitless in view of the expressions for $S_{\pm}^{\rm hs,ls}$ given in (18b) and (19b).

In an analogous fashion for the phase, it follows from (48), the "+" instance of (18b), and arguments similar to the ones used to prove (49), that

$$\hat{V}_{ic}\frac{d\phi_{oc}^{\rm hs}}{d\hat{V}_{ic}} = \pm 2\left\{\left(S_{+}^{\rm hs}\right)^2 - \left[\frac{1+\left(S_{+}^{\rm hs}\right)^2 - \left(S_{-}^{\rm hs}\right)^2}{2}\right]^2\right\}^{1/2} \tag{53}$$

where $\phi_{oc}^{\rm hs}$ denotes the output carrier phase relative to θ_B for high-side injection [see (18a)]. Similar to the convention for AM/AM, it is customary to calculate and report AM/PM values in degrees/decibel. Using (51), (53) can be written

$$\frac{d\phi_{oc}^{\rm hs}(\rm deg)}{d\hat{V}_{ic}(\rm dB)} = \pm\frac{18\ln 10}{\pi}\left\{\left(\tilde{S}_{+}^{\rm hs}\right)^2 - \left[\frac{1+\left(\tilde{S}_{+}^{\rm hs}\right)^2 - \left(\tilde{S}_{-}^{\rm hs}\right)^2}{2}\right]^2\right\}^{1/2} \tag{54a}$$

and, similarly, for the low-side injection case by

$$\frac{d\phi_{oc}^{\rm ls}(\rm deg)}{d\hat{V}_{ic}(\rm dB)} = \pm\frac{18\ln 10}{\pi}\left\{\left(\tilde{S}_{-}^{\rm ls}\right)^2 - \left[\frac{1+\left(\tilde{S}_{-}^{\rm ls}\right)^2 - \left(\tilde{S}_{+}^{\rm ls}\right)^2}{2}\right]^2\right\}^{1/2} \tag{54b}$$

where $\tilde{S}_{\pm}^{\rm hs,ls}$ is as in (52), and the sign $\pm$ is left undetermined (although it is known that these derivatives are continuous with respect to $\hat{V}_{ic}$, and that they are zero in the linear regime of operation [see (6)]).

The last determination to be made here is that of the dynamic carrier conversion curves

$$\hat{V}_{oc}^{\rm hs,ls} = \hat{V}_{oc}^{\rm hs,ls}\left(\hat{V}_{ic}, \Delta f\right)$$

and

$$\phi_{oc}^{\rm hs,ls} = \phi_{oc}^{\rm hs,ls}\left(\hat{V}_{ic}, \Delta f\right)$$

from the measurements of $S_{\pm}^{\rm hs,ls} = S_{\pm}^{\rm hs,ls}(\hat{V}_{ic}, \Delta f)$. Again, only treating the high-side injection case with any detail, we return to (50) and rewrite it as follows for a fixed value of Δf:

$$\frac{d\hat{V}_{oc}^{\rm hs}}{\hat{V}_{oc}^{\rm hs}} = \left[\left(S_{+}^{\rm hs}\right)^2 - \left(S_{-}^{\rm hs}\right)^2\right]\frac{d\hat{V}_{ic}}{\hat{V}_{ic}} \tag{55}$$

so that, by indefinite integration, we find that

$$\hat{V}_{oc}^{\rm hs}\left(\hat{V}_{ic}, \Delta f\right) = e^{\kappa}e^{\nu^{\rm hs}(\hat{V}_{ic}, \Delta f)} \tag{56a}$$

where κ is an integration constant and

$$\nu^{\rm hs}\left(\hat{V}_{ic}, \Delta f\right) := \int \frac{\left[S_{+}^{\rm hs}\left(\hat{V}_{ic}, \Delta f\right)\right]^2 - \left[S_{-}^{\rm hs}\left(\hat{V}_{ic}, \Delta f\right)\right]^2}{\hat{V}_{ic}} d\hat{V}_{ic}. \tag{56b}$$

Applying the small-signal condition (6) to (56a) and solving for e^{κ}, the dynamic carrier amplitude conversion is given by

$$\hat{V}_{oc}^{\rm hs}\left(\hat{V}_{ic}, \Delta f\right) = G_s V_{ic}^r e^{[\nu^{\rm hs}(\hat{V}_{ic}, \Delta f) - \nu^{\rm hs}(V_{ic}^r, \Delta f)]} \tag{57a}$$

and, similarly, for the low-side injection case (hs $\rightarrow$ ls), with

$$\nu^{\rm ls}\left(\hat{V}_{ic}, \Delta f\right) := \nu^{\rm hs}(\hat{V}_{ic}, \Delta f)\Big|_{S_{\pm}^{\rm hs} \rightarrow S_{\mp}^{\rm ls}} \tag{57b}$$

instead. In both cases, $V_{ic}^r = |H_1(f_c)|A = A/A_{\max}$ assuming (24) holds.

Proceeding in a similar manner for $\phi_{oc}^{\rm hs}$, it follows from (53) that

$$\phi_{oc}^{\rm hs}\left(\hat{V}_{ic}, \Delta f\right) = \Phi^{\rm hs}\left(\hat{V}_{ic}, \Delta f\right) + \kappa \tag{58a}$$

where κ is an integration constant and

$$\Phi^{\rm hs}(\hat{V}_{ic}, \Delta f) := \pm 2\int\left\{\left(S_{+}^{\rm hs}\right)^2 - \left[\frac{1+\left(S_{+}^{\rm hs}\right)^2 - \left(S_{-}^{\rm hs}\right)^2}{2}\right]^2\right\}^{1/2}\frac{d\hat{V}_{ic}}{\hat{V}_{ic}}. \tag{58b}$$

Imposing a small-signal condition, as done above for $V_{oc}^{\rm hs}$, the constant κ in (58a) can be determined so that the dynamic carrier phase conversion is given by

$$\phi_{oc}^{\rm hs}\left(\hat{V}_{ic}, \Delta f\right) = \phi_s + \Phi^{\rm hs}\left(\hat{V}_{ic}, \Delta f\right) - \Phi^{\rm hs}\left(V_{ic}^r, \Delta f\right) \tag{59a}$$

and, similarly, for the low-side injection case (hs $\rightarrow$ ls), with

$$\Phi^{\rm ls}\left(\hat{V}_{ic}, \Delta f\right) := \Phi^{\rm hs}(\hat{V}_{ic}, \Delta f)\Big|_{S_{\pm}^{\rm hs} \rightarrow S_{\mp}^{\rm ls}} \tag{59b}$$

instead, and in both cases, V_{ic}^r is as above.

III. Measurement Procedure and Precautions

As discussed above, the test system described here can obtain dynamic AM/AM and AM/PM from measurements of only intermodulation product amplitudes [9]. Since no phase measurements are required, the test equipment requirements are simpler and less costly than those used in the VNA-based static approach. A block diagram of the measurement setup is shown in Fig. 2. The input signal to the power-amplifier device-under-test (DUT) consists of two CW tones, one at $f_c \pm \Delta f$ being 20–30 dB smaller than the other tone at f_c. The output signal would consist of tones only at the two input frequencies if the DUT were linear. In a nonlinear DUT, AM/AM and AM/PM conversion generates an intermodulation product at $f_c \mp \Delta f$. In order to deembed the two filters for the three-box model, however, several additional measurements are necessary, depending on the approaches outlined above. Such measurements include small-signal VNA sweeps across the power-amplifier passband, moving the aforementioned two tone across the same passband and locating its maximum carrier output and corresponding phase shift, or possibly even

time-domain measurements and Fourier analysis in order to obtain the necessary phase shifts in the large-signal regime. With the gain of $H_2(f)$ in hand, the amplitude measurements of the two input tones and of the three output tones for both injection cases yield all the information required to calculate the dynamic AM/AM and AM/PM conversions.

To derive the dynamic AM/AM and AM/PM, a reference measurement is first made where the input tones are reduced in power to the point that the DUT is in linear operation. Six reference measurements are made: the input voltage V_{ic}^r at f_c, the input voltage $V_{i\pm}^r$ at $f_c \pm \Delta f$, the output voltage V_{oc}^r at f_c, and the output voltage $V_{o\pm}^r$ at $f_c \pm \Delta f$. The input tones are then increased in power to the desired operating point. Eight additional measurements are made: the input voltage V_{ic} at f_c, the input voltage $V_{i\pm}$ at $f_c \pm \Delta f$, the output voltage $V_{oc}^{\mathrm{hs,ls}}$ at f_c, the output voltages $V_{o\pm}^{\mathrm{hs}}$ at $f_c \pm \Delta f$ for high-side injection, and the output voltages $V_{o\pm}^{\mathrm{ls}}$ at $f_c \pm \Delta f$ for low-side injection. Having all these measurements, the ratios in (8) and (22) can be easily calculated. The next step is to then calculate $|H_2(f)|$ using either of two procedures described in Section II-B.1. The normalized output amplitudes of the sidebands, denoted by $S_{\pm}^{\mathrm{hs,ls}}$ at the frequency $f_c \pm \Delta f$ can then be obtained from (23). The dynamic AM/AM (decibels/decibel) and AM/PM (degrees/decibel) are then calculated from (52) and (54), respectively, while the dynamic AM/AM conversion curves are obtained from (56b) and (57), and the dynamic AM/PM conversion curves are obtained from (58b) and (59).

Since (23) involves amplitude ratios of signals at the same frequency, the two-tone dynamic technique does not require that the microwave components (e.g., couplers) or the microwave instruments (e.g., power sensors, spectrum analyzer, signal generators) have a flat frequency response. In addition, since (23) involves only amplitude ratios, absolute power measurements are not required. However, it is essential that the power sensors and spectrum analyzer have excellent linearity. Fortunately, power sensors, when operated somewhat below their maximum power input, have negligible deviation from linearity. The spectrum analyzer is not as linear, but can be made acceptable by following certain precautions. First, spectrum analyzer settings other than the center frequency must not be changed in the course of the measurement sequence. Changing the resolution bandwidth, for instance, can change the power reading by a few tenths of a decibel, which is unacceptable. Second, the spectrum analyzer power readings should be linearized by means of a lookup table. The table can be generated by a comparison between spectrum analyzer measurements and power meter measurements. Third, the video bandwidth and other settings should be such that spectrum analyzer readings are consistent from sweep to sweep. Automation of the lookup-table generation, as well as the main measurement sequence, was implemented in the *LabVIEW* application.[3]

Note that (54), which is used to derive dynamic AM/PM, is sensitive to small errors for low AM/PM values. For instance, if the AM/PM is only 0.9°/dB, then an error in the measurement of the normalized sideband amplitudes of 0.09 dB can yield 100% error in this value. In contrast, if the AM/PM is 4°/dB, then an error in the normalized sideband amplitudes of 0.1 dB yields less than 5% error in the AM/PM value. Note that, in devices with low AM/PM, nearly all the signal distortion is caused by the AM/AM curve, so the two-tone technique can still be used as a means to generate a dynamic AM/AM curve, even though the AM/PM results will be subject to large error.

This technique may not be applicable for all types of power amplifiers. Erroneous results may be obtained for power amplifiers having more than one nonlinearity (e.g., a multistage amplifier with more than one saturating stage or an amplifier containing saturated devices in parallel).

[3]*LabVIEW*, Virtual Instrumentation Software, National Instrumentation Corporation, Austin, TX.

IV. Measurement Results and Discussion

This section of the paper provides measured results for amplifiers that are typical of those used in microwave communication systems. Measured results and validation is included for both SSA and TWTA devices. A simple one-box version of the full three-box model is constructed for an SSA from two-tone measurements. Good agreement is obtained between the model and intermodulation product measurement over a wide range of input levels. A TWTA is measured in the following three ways:

1) statically with the network analyzer;
2) dynamically with the two-tone technique;
3) dynamically with a 16 quadrature-amplitude-modulation (QAM) technique.

Good agreement is found between all three techniques for AM/AM conversion. A significant difference is noted between the static and dynamic techniques for AM/PM conversion. The application of the two-tone technique is also extended to obtain the amplitude characteristics of a TWTA output filter.

A. SSA Measurement Results

This section presents the dynamic AM/AM and AM/PM conversions for an SSA (DBS Model 028N315). In this example, the large tone at f_c was at 2.8 GHz and the offset tone was at 2.81 GHz (25 dB smaller than the large tone). Treating the SSA as a nonlinear one-box, we see from (23) that the sideband amplitude components $S_{\pm}^{\mathrm{hs,ls}}$ can be calculated using only small- and large-signal spectrum analyzer and power-meter measurements. These quantities can then be substituted into (52) and (54), and then numerically integrated to arrive at the dynamic AM/AM and AM/PM conversion curves shown in Fig. 3.

To check the validity of these results, a comparison of the output distortion was made between the one-box model predictions and the measured results. This was performed for a two-tone input signal over a 20-dB power range. The tones were separated by 10 MHz and the first-tone input power was at 6-dB input backoff from saturation. The second-tone input power was swept from 26- to 6-dB backoff from saturation. Fig. 4 shows how well the model predicts the output level of the tones and the third- and fifth-order intermodulation products. Even though the model was generated from third-order intermodulation measurements using a two-tone input with a 25-dB difference in power level, it accurately predicts not only the output for two tones of equal magnitude, but also the magnitude of the fifth-order intermodulation products.

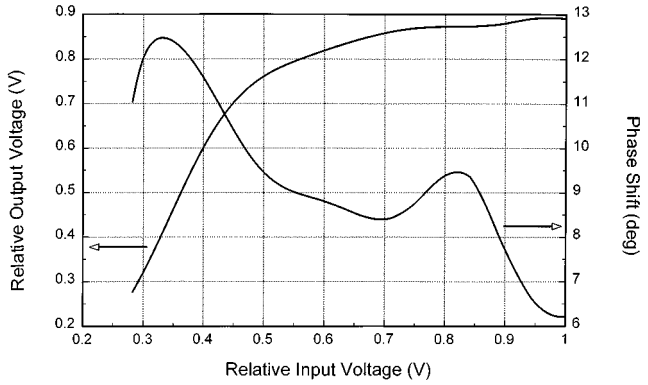

Fig. 3. Measurement-based SSA dynamic AM/AM and AM/PM conversions.

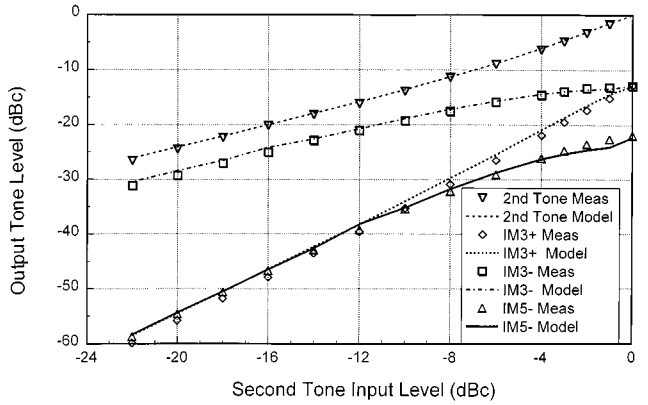

Fig. 4. Modeled versus measured SSA distortion characteristics.

B. TWTA Measurement Results

This section presents the measurement of AM/AM and AM/PM for a TWTA (Hughes Model 1277H) operating at 1.65 GHz. To contrast the differences between static and dynamic measurements, AM/AM and AM/PM curves were measured using the following three methods:

1) standard static VNA technique;
2) two-tone dynamic technique with an offset frequency of 0.5 MHz;
3) another dynamic technique using a 16-QAM input signal.

The 16-QAM dynamic method used a signal at a symbol rate of 1 MHz, conveniently generated by an HP8780A vector signal generator, and demodulated by an HP8981A vector modulation analyzer. This setup is shown in Fig. 5, where the mixers are needed because of the modulation analyzer's 200-MHz carrier limit.

The 16-QAM signal was sent through the TWTA. A reference measurement was first made with the TWTA in linear operation, then the signal level was increased to the desired operating point. The phase rotation and amplitude compression of the outer 12 constellation points was compared to the inner four points to derive the AM/PM and AM/AM with the reference measurement being used to correct for the nonideality of the modem. The HP 8981A has A/D converters that can digitize the constellation points, simplifying the calculations. Since this QAM measurement is also a dynamic technique, the results are expected to agree more closely with the two-tone dynamic technique than the VNA static technique.

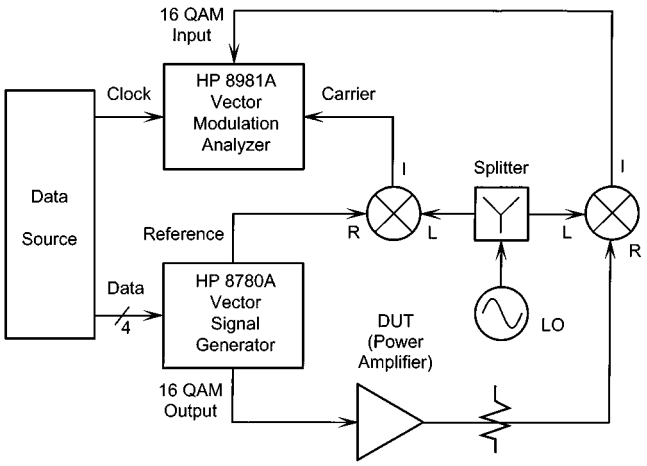

Fig. 5. 16-QAM dynamic AM/AM, AM/PM test configuration.

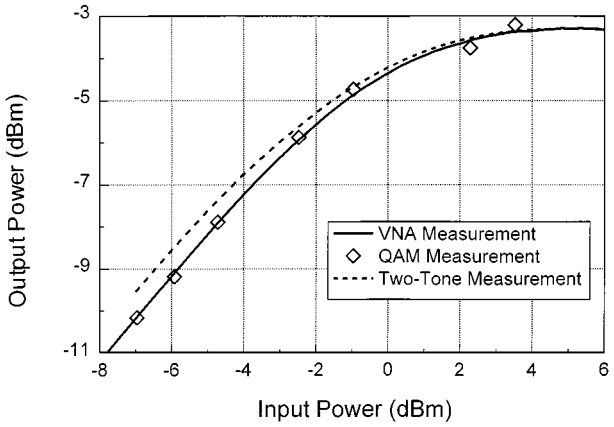

Fig. 6. Comparison of TWTA AM/AM measurement results.

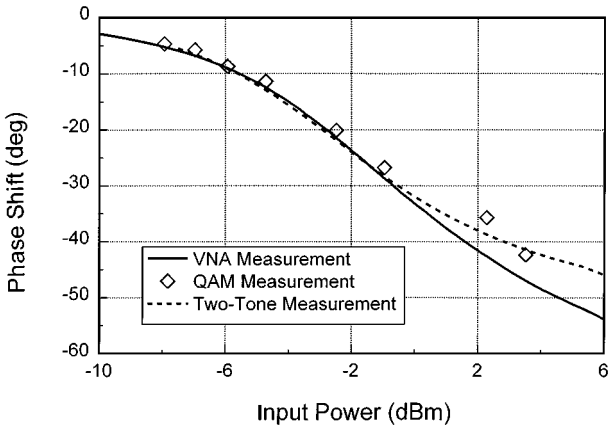

Fig. 7. Comparison of TWTA AM/PM measurement results.

The results shown in Figs. 6 and 7 demonstrate that the 16-QAM and two-tone techniques do indeed exhibit better agreement than either one does with the VNA measurement, particularly for the phase shift versus input power. The dynamic AM/PM of this TWTA may be lower than its static value due to the dynamics of the power supply as it is driven into saturation. A settling time of several milliseconds was observed when the TWTA was driven with a stepped input signal.

The two-tone measurements described previously used a fixed offset frequency for the small-signal tone. The SSA

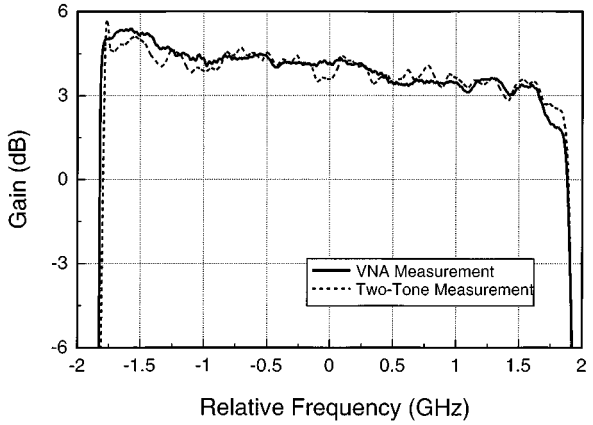

Fig. 8. Comparison of TWTA output filter amplitude response obtained from VNA and two-tone measurements.

measurements used an offset frequency of 10 MHz and the TWTA measurements used an offset frequency of 0.5 MHz. In both cases, the offset frequency is small enough that the effects of the input and output filters in the three-box model are insignificant. In order to test the three-box model, including the two filters, a set of measurements were performed where the offset frequency and center frequency were simultaneously stepped across a 2.0-GHz bandwidth. These measurements were performed on a higher frequency broad-band TWTA having an external output filter. A 100 different frequency points were measured, and the amplitude response of the output filter $H_2(f)$ was calculated according to (29) and the procedure described afterwards. Fig. 8 shows the result and, for comparison, it includes a VNA measurement of the output filter external to the TWTA that was present in the measurements. The VNA measurement and the two-tone measurement are similar, but do not completely agree. The VNA and two-tone measurements are expected to agree within measurement error only if there was no output filter $H_2(f)$ internal to the TWTA.

V. Conclusion

This paper has presented a simple two-tone technique to measure the dynamic carrier AM/AM and AM/PM curves of a nonlinear device. A complete two-tone signal analysis showed how these curves can be derived from the amplitude measurement of intermodulation products. Thus, a nonlinear one- or three-box model can be constructed using a carrier dynamically modulated at rates consistent with real-world applications. This is an enhancement to models based on static carrier measurements, which could be in error due to thermal or dc-bias effects. The one-box model can be directly constructed from spectrum analyzer and power meter measurements made under small- and large-signal two-tone excitations. The three-box model requires additional small-signal VNA sweeps, and large-signal time-domain measurements, in order to obtain the amplitude and phase responses of the surrounding filters. A comprehensive and formal identification of several possible versions of the three-box model was provided, including the details of the measurement and data-processing procedures needed to arrive at the model components.

A practical implementation of this technique has been described, including the precautions necessary for accurate results. Measurements were first presented for an SSA. These measurements were validated by demonstrating the ability to predict intermodulation products out to fifth order over a wide range of input levels using a one-box dynamic AM/AM and AM/PM model. In addition, measurements of a TWTA were presented where the two-tone derived dynamic curves differed from the single-tone derived static curves. The dynamic measurement was validated by comparison to a measurement of the distortion of a 16-QAM input constellation.

Acknowledgment

The authors would like to thank Dr. J. D. Michaelson, Dr. K. M. Soo Hoo, and Dr. J. H. Spriggs, The Aerospace Corporation, El Segundo, CA, for their generous support and guidance during the primary development of this paper.

References

[1] R. M. Gagliardi, *Satellite Communications*, 2nd ed. New York: Van Nostrand, 1991.
[2] L. L. Larson, Ed., *RF and Microwave Circuit Design for Wireless Communications*. Norwood, MA: Artech House, 1996.
[3] M. C. Jeruchim, P. Balaban, and K. S. Shanmugan, *Simulation of Communication Systems: Modeling, Methodology, and Techniques*, 2nd ed. Norwell, MA: Kluwer, 2000.
[4] O. Shimbo, "Effects of intermodulation, AM-PM conversion and additive noise in multicarrier TWT systems," *Proc. IEEE*, vol. 59, pp. 230–238, Feb. 1971.
[5] S. Ariyavistakul and T.-P. Liu, "Characterizing the effects of nonlinear amplifiers on linear modulation for digital portable radio communications," *IEEE Trans. Veh. Technol.*, vol. 39, pp. 383–389, Nov. 1990.
[6] J. S. Kenney and A. Leke, "Power amplifier spectral regrowth for digital cellular and PCS applications," *Microwave J.*, vol. 38, no. 10, pp. 74–92, Oct. 1995.
[7] A. L. Berman and C. E. Mahle, "Nonlinear phase shift in traveling-wave tubes as applied to multiple access communications satellites," *IEEE Trans. Commun. Technol.*, vol. COM-18, pp. 37–47, Feb. 1970.
[8] A. A. M. Saleh and D. C. Cox, "Improving the power aided efficiency of FET amplifiers operating with varying envelope signals," *IEEE Trans. Microwave Theory Tech.*, vol. MTT-31, pp. 51–56, Jan. 1983.
[9] J. P. Laico, H. L. McDowell, and C. R. Moster, "A medium power traveling-wave tube for 6000-Mc radio relay," *Bell Syst. Tech. J.*, vol. 35, no. 6, pp. 1285–1346, Nov. 1956.
[10] S. A. Maas, *Nonlinear Microwave Circuits*. Norwood, MA: Artech House, 1988.
[11] J. F. Sevic and M. B. Steer, "Analysis of GaAs MESFET spectrum regeneration driven by a $\pi/4$-DQPSK modulated source," in *IEEE MTT-S Int. Microwave Symp. Dig.*, May 14–19, 1995, pp. 1375–1378.
[12] N. M. Blachman, "Bandpass nonlinearities," *IEEE Trans. Inform. Theory*, vol. IT-10, pp. 162–164, Apr. 1964.
[13] E. D. Sunde, *Communication Systems Engineering Theory*. New York: Wiley, 1969.
[14] N. M. Blachman, "Detectors bandpass nonlinearities and their optimization: Inversion of the Chebyshev transform," *IEEE Trans. Inform. Theory*, vol. IT-17, pp. 398–404, July 1971.
[15] A. R. Kaye, D. A. George, and M. J. Eric, "Analysis and compensation of bandpass nonlinearities for communications," *IEEE Trans. Commun.*, vol. COM-20, pp. 965–972, Oct. 1972.
[16] A. Leke and J. S. Kenney, "Behavioral modeling of narrowband microwave power amplifiers with applications in simulating spectral regrowth," in *IEEE MTT-S Int. Microwave Symp. Dig.*, June 16–21, 1996, pp. 1385–1388.
[17] A. A. M. Saleh, "Frequency-independent and frequency-dependent nonlinear models of TWT amplifiers," *IEEE Trans. Commun.*, vol. COM-29, pp. 1715–1720, Nov. 1981.
[18] A. A. Moulthrop, M. S. Muha, C. P. Silva, and C. J. Clark, "A new time-domain measurement technique for microwave devices," in *IEEE MTT-S Int. Microwave Symp. Dig.*, vol. 2, Baltimore, MD, June 7–12, 1998, pp. 945–948.
[19] M. S. Muha, C. J. Clark, A. A. Moulthrop, and C. P. Silva, "Accurate measurement of wideband modulated signals," *Microwave J.*, vol. 43, pp. 84–98, June 2000.
[20] M. Schwartz, W. R. Bennet, and S. Stein, *Communication Systems and Techniques*. New York: McGraw-Hill, 1966.

Christopher J. Clark was born in Washington, DC, in 1960. He received the B.S.E.E. and M.S.E.E. degrees from the University of Maryland at College Park, in 1983 and 1986, respectively.

From 1984 to 1986, he was with the Watkins-Johnson Company, where he was responsible for the design and development of RF receiving systems. From 1986 to 1992, he was with TRW Inc., where he developed microwave components for satellite applications. His primary focus was in the design of MESFETs, high electron-mobility transistors (HEMTs), and heterojunction bipolar transistor (HBT) GaAs monolithic microwave integrated circuits (MMICs) for phased-array systems. From 1992 to 1999, he was with The Aerospace Corporation, where he was involved with the design of space communication systems and development of hardware for digital satellite applications. He is currently a Principal Engineer with the Multilink Technology Corporation, Santa Monica, CA, where he is involved with the design and development of high-speed electronics for use in major commercial optical communication systems.

Mr. Clark is a member of Eta Kappa Nu and Tau Beta Pi.

Christopher P. Silva (S'81–M'82–SM'98–F'99) was born on March 17, 1960, in Fortuna, CA. He received the B.S., M.S., and Ph.D. degrees from the University of California at Berkeley, in 1982, 1985, and 1993, respectively, all in electrical engineering.

He was a Post-Graduate Researcher with the Electronics Research Laboratory, University of California at Berkeley, where he investigated the chaotic dynamics of nonlinear circuits and systems. In 1989, he joined the Electronics Research Laboratory, The Aerospace Corporation, Los Angeles, CA, where he is currently an Engineering Specialist in the Electromagnetic Techniques Department, Electronic Systems Division. He has been the Principal Investigator on several internally funded research projects addressing nonlinear microwave computer-aided design (CAD), secure communications by means of chaos, and the modeling and compensation of nonlinear satellite communications channels, the latter of which has evolved into a program support effort for advanced satellite communications technology development. He has given many invited conference, society meeting, and other outside institution talks on the latter two subjects, along with having authored or co-authored corresponding publications.

Dr. Silva is a member of Eta Kappa Nu, Tau Beta Pi, Phi Beta Kappa, the Society for Industrial and Applied Mathematics, the American Mathematical Society, and the American Association for the Advancement of Science. He is a senior member of the American Institute for Aeronautics and Astronautics. He was the recipient of a National Science Foundation Fellowship and a Lockheed Leadership Fellowship.

Andrew A. Moulthrop was born in San Francisco, CA, in 1955. He received the B.A. degree in physics from the University of California at San Diego, La Jolla, in 1977, and the Ph.D. degree in physics from the University of California at Berkeley, in 1984.

He was a Research Assistant with the University of California at Berkeley, where he co-developed a Josephson junction parametric amplifier, as well as measured various properties of superfluid helium. He is currently a Senior Engineering Specialist in the Electromagnetic Techniques Department, Electronic Systems Division, The Aerospace Corporation, Los Angeles, CA, where he is involved with the design, development, and measurement of microwave components and systems.

Dr. Moulthrop is a member of Phi Beta Kappa.

Michael S. Muha was born in Inglewood, CA, on February 21, 1958. He received the B.S. degree in physics from the University of Southern California, Los Angeles, in 1979, and the M.S. degree in applied physics from the California Institute of Technology, Pasadena, in 1981.

While with the California Institute of Technology, he was involved with the design and development of millimeter-wave and far-infrared imaging antenna arrays. He is currently a Senior Engineering Specialist with the Electromagnetic Techniques Department, Electronic Systems Division, The Aerospace Corporation, Los Angeles, CA, where he is involved with the design, development, and characterization of high-data-rate microwave communications systems.

Mr. Muha is a member of Phi Beta Kappa and Phi Kappa Phi.